Rotational Stabilization of Resistive Wall Modes by the Shear Alfvén Resonance

L.-J. Zheng,[1,*] M. Kotschenreuther,[1] and M. S. Chu[2]

[1]*Institute for Fusion Studies, University of Texas at Austin, Austin, Texas 78712, USA*
[2]*General Atomics, P.O. Box 85608, San Diego, California 92186, USA*

(Received 28 February 2005; published 16 December 2005)

It is found that resistive wall modes with a toroidal number $n = 1$ in tokamaks can be stabilized by plasma rotation at a low Mach number, with the rotation frequency being lower than the ion bounce frequency but larger than the ion and electron precession drift frequencies. The stabilization is the result of the shear-Alfvén resonance, since the thermal resonance effect is negligible in this rotation frequency range. This indicates that tokamaks can operate at normalized pressure values beyond the no-wall stability limit even for low values of plasma rotation, such as those expected in fusion reactor scale devices.

DOI: 10.1103/PhysRevLett.95.255003 PACS numbers: 52.35.Py, 52.55.Fa, 52.55.Hc

Resistive-wall-mode (RWM) stability is important for tokamak confinement [1]. Experimentally, it was observed that plasma rotation can stabilize resistive wall modes [2–4]. Theoretically, it was found that mode coupling to the sound wave resonance in rapidly rotating plasmas can lead to stabilization of resistive wall modes [5–7]. The precession drift resonance in a slowly rotating plasma was likewise shown to be a stabilizing mechanism [8]. The interaction of plasma rotation with plasma dissipation can also result in resistive-wall-mode stabilization [9,10].

In this Letter we show that the shear-Alfvén resonance in rotating plasmas by itself can lead to full stabilization of resistive wall modes. Previously, the shear-Alfvén continuum damping of the resistive-wall mode was investigated in a cylindrical model with the zero-pressure singular layer equation [11,12]. However, the strength of the continuum damping needs to be assessed in toroidal geometry with finite-pressure for realistic devices, such as the International Thermonuclear Experimental Reactor (ITER) [13]. This requires numerical computation.

Moreover, the calculation of the shear-Alfvén continuum damping requires a sophisticated numerical method. In previous calculation for toroidal Alfvén eigenmodes, a technique based on changing the radial integration orbit from the real orbit to a complex one surrounding the Alfvén singularities was used to calculate the continuum damping [14]. In this Letter we show that adaptive shooting together with a small-growth-rate treatment is an alternative technique. The small-growth-rate method needs very high resolution computation near the singularities. The adaptive numerical scheme of our AEGIS (Adaptive EiGenfunction Independent Solution) code overcomes this difficulty [15]. The AEGIS adaptive numerical scheme has advantages in this regard over nonadaptive codes, such as MARS [5]. In the calculations with the MARS code [5,6], Bondeson and Ward concluded that the rotation stabilization is primarily a bulk plasma effect associated with the Landau damping of sound waves coupled to the instability. The bulk nature of the damping is due to the fact that the mode drives sound waves through toroidal coupling, so that these waves are primarily nonresonant sidebands. The sidebands do, however, play a role in the vicinity of the singular layers through the so-called apparent mass effect [16]. Bondeson and Ward examined the role of shear-Alfvén resonant damping near the singular layers and incorrectly concluded that it was insignificant [6]. Subsequent investigations with the MARS code thus emphasized the bulk Landau damping. The present work, however, shows that shear-Alfvén damping is large and can be the dominant effect for low plasma rotation.

In order to isolate the shear-Alfvén resonance damping effect, we consider the following frequency regime:

$$\omega_b \gg \Omega \gg \langle \omega_d \rangle_b, \tag{1}$$

where Ω is the rotation frequency, ω_b is the ion bounce frequency, and $\langle \omega_d \rangle_b$ denotes the bounce-averaged magnetic drift frequency. In this frequency regime the particle-wave thermal resonances are very small. An even more important reason to consider the frequency regime in Eq. (1) is that it applies to the current design of ITER, for which rotation is expected to have low Mach number.

The equilibrium is generated numerically with the TOQ equilibrium code. The AEGIS code reads the TOQ equilibrium data and performs the stability analysis. We investigated ITER-like configurations with the following parameters: major radius 6.2 m, minor radius 2.0 m, elongation of the plasma cross section 1.86, and triangularity 0.5. The safety factor at the 95% flux surface is $q_{95} = 3$. We take the value of the safety factor at the magnetic axis, q_0, to be 1.05, slightly above unity, even though q_0 is below unity in the ITER design. In this configuration the no-wall stability limit occurs at $\beta_{N,\mathrm{crit}} = 3.4$, where $\beta_N = \beta(I/aB_0)^{-1}$ with I the toroidal current, a the minor radius, B_0 the magnetic field at the magnetic axis, corresponding to a volume-averaged beta value of $\langle \beta \rangle_{\mathrm{crit}} = 5.5\%$. Here, β represents the ratio of the plasma and magnetic pressures. We raised q_0 slightly above unity in order to avoid the excitation of internal kink modes. Consequently, the marginal beta values in this configuration are higher than those for the ITER design (viz., $\beta_{N,\mathrm{crit}} = 1.77$ and $\langle \beta \rangle_{\mathrm{crit}} = 2.5\%$). To examine the rotational effect on resis-

tive wall modes, we investigate an equilibrium with beta values $\beta_N = 3.88$ and $\langle\beta\rangle = 6.2\%$, which are above the marginal no-wall stability values. The critical position of a perfectly conducting wall for stabilizing the resistive wall modes in this equilibrium is at $b = 1.53$, where b is the wall position.

To study the rotational effect on the resistive wall modes in the frequency regime given in Eq. (1), the following equation for toroidal plasma was solved with the AEGIS code:

$$-\rho(1+M_\parallel)(\omega+n\Omega+i\gamma_p)^2\boldsymbol{\xi}_\perp = \nabla(\boldsymbol{\xi}_\perp\cdot\nabla P)+\mathbf{J}\times\mathbf{Q} + (\nabla\times\mathbf{Q})\times\mathbf{B}. \quad (2)$$

Here, $\boldsymbol{\xi}_\perp$ represents the magnetic field line displacement, with subscript $\perp$ denoting the component perpendicular to the equilibrium magnetic field $\mathbf{B}$; $\mathbf{Q} = \nabla\times(\boldsymbol{\xi}_\perp\times\mathbf{B})$ is the perturbed magnetic field; n is the toroidal mode number; $\mathbf{J}$ denotes the equilibrium current density; P is the equilibrium plasma pressure; and ρ denotes the plasma mass density. The effects of parallel inertia, Coriolis force, and plasma compressibility do not appear explicitly in Eq. (2); they are replaced by the so-called apparent mass effect $M_\parallel$, which is simply given by $M_\parallel = 2q^2$ in the case of large aspect ratio and circular cross section [16]. The structure of Eq. (2) is also justified from a fully gyrokinetic treatment [17,18], which yields a further enhancement of the apparent mass effect by the square root of the aspect ratio, due to the contribution from particles with small parallel velocities. In the present study, we do not use kinetic theory to compute the kinetic enhancement of the apparent mass $M_\parallel$, but simply take the magnitude of $M_\parallel$ to be enlarged by the square root of the aspect ratio and define the Alfvén frequency using the total mass density $\rho(1+M_\parallel)$. The simple structure of Eq. (2) results from the low frequency ordering in Eq. (1). In this frequency ordering the particle-wave resonance effects are negligible, and the centrifugal force effect can also be ignored [17]. The rotation effect is negligible in the bulk plasma and becomes important only in the vicinity of the mode resonance layers: $x^2 - (\omega_r + n\Omega)^2 = 0$, where x is the normalized distance from the rational surface and ω_r is the real part of the mode frequency. In Eq. (2) γ_p is a small positive parameter taken to approach zero, which we use to heal the numerical singularity while calculating the Alfvén damping. This technique is similar to that used to evaluate Landau damping with a small imaginary parameter. For sufficient small γ_p, the numerical result is insensitive to the value of γ_p. The solution of Eq. (2) is then matched to the vacuum and wall solutions to form a complete eigenvalue problem. The thin-wall assumption is adopted in our investigation.

The numerical study of the eigenvalue problem shows that plasma rotation can be a substantial stabilization mechanism for resistive wall modes, even when Alfvén resonances are the only dissipation. Figure 1 shows the dependence of the growth rate of the $n = 1$ mode on the wall position b for the ITER-type equilibrium described previously. Figure 1 shows that the resistive-wall-mode growth rate initially increases as the wall position increases. However, after a certain wall position, the growth rate drops sharply and the resistive wall modes become stable. The most unstable resistive wall modes are found to be those with negligibly small ω_r, consistent with the previous numerical result [6]. This is because for an oscillating magnetic field with finite frequency, the resistive wall behaves like a conducting wall due to the skin effect. Therefore, the resistive wall modes with finite frequency are usually stable. The most unstable case is always the case with negligibly small mode frequency. The dependence of the growth rate on the plasma rotation frequency for fixed b can also be deduced from Fig. 1. For a fixed wall position, the growth rate first increases as the rotation frequency increases and then decreases as the rotation frequency increases further. The growth rate vanishes at a sufficiently large plasma rotation frequency. The stability region in terms of the wall position and the rotation frequency is plotted in Fig. 2. The region $b < 1.53$ is stable for a perfectly conducting wall, but unstable for resistive wall modes without plasma rotation. In the presence of plasma rotation, a stable region appears. It is informative to plot the eigenmode structure. Figures 3 and 4 display the real and imaginary parts of the eigenmodes when the rotation frequency is $\Omega = 0.005$, with ξ_ψ the component of $\boldsymbol{\xi}_\perp$ perpendicular to magnetic flux surface ψ.

We now justify our numerical results in three respects. First, we note that the rotational effect in Eq. (2) does not alter the basic equation structure, except to make the problem complex. Therefore, as a check of our code, the numerical results in the limit $\Omega = 0$ were compared with the results computed from the GATO code [19]. We con-

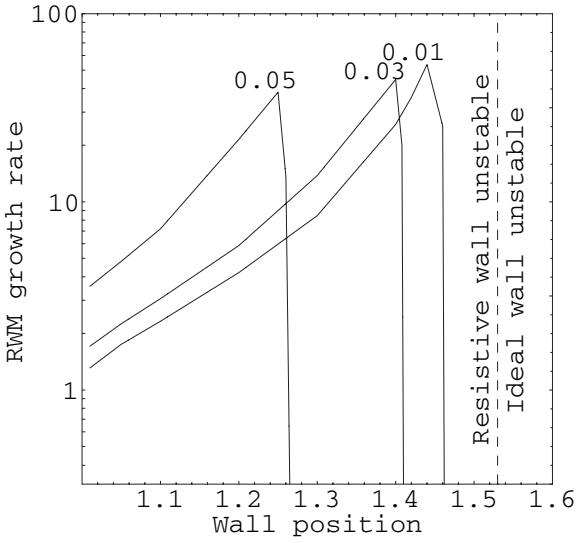

FIG. 1. RWM growth rate versus wall position with plasma rotation frequency (normalized by the Alfvén frequency counting in the apparent mass effect) as a parameter.

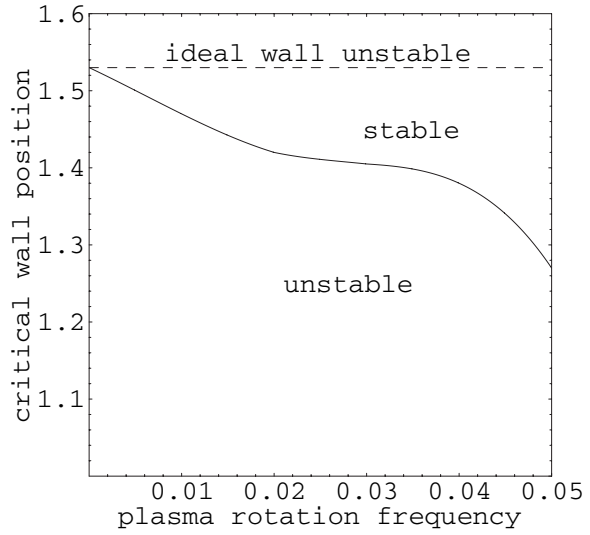

FIG. 2. Stability boundary as a function of the critical wall position and the normalized plasma rotation frequency.

firmed that, in this limit, the real part of the eigenmode (shown in Fig. 3) reduces to the usual ideal MHD solution, which agrees completely with the GATO result, and the imaginary part simply vanishes.

Second, since the main rotational modification of the eigenmodes appears only in the vicinity of the mode singular layers, we compared the numerical solutions near the singular layers with the analytical solutions. Near the singular layers, the mode can be described by the singular layer equation [16]

$$\frac{d}{dx}[x^2 - (\omega_r + n\Omega + i\gamma_p)^2]\frac{d\xi_\psi}{dx} = 0, \qquad (3)$$

where the finite β effect is dropped for simplicity. The solution of Eq. (3) is

$$\xi_\psi = -i\xi_\psi^l \ln\frac{x - (\omega_r + n\Omega) - i\gamma_p}{x + (\omega_r + n\Omega) + i\gamma_p} + \xi_\psi^s, \qquad (4)$$

where ξ_ψ^l and ξ_ψ^s are constants describing the so-called large and small solutions, respectively. The solution in Eq. (4) has multiple values. Branch cuts must be imposed. From the causality condition one can prove that the cuts should be from the poles at $x = \pm(\omega_r + n\Omega + i\gamma_p)$ to ∞, respectively. With these cuts introduced, ξ_ψ becomes single valued. The plasma rotation splits each MHD singular layer at $x = 0$ into twin layers at $x = \pm(\omega_r + n\Omega)$. The value of the real part of ξ_ψ jumps by π across each of the twin layers and is flat between. These characteristics near the singular layers can be seen in our numerical solutions (Fig. 3). Equation (4) shows that the imaginary part of ξ_ψ is a sum of two shifted logarithm peaks in opposite signs; Fig. 4 shows exactly this feature. The resemblance between analytical and numerical results extends to all other rotation frequencies. Because of space limitations, only one set of numerical global eigenmodes for $\Omega = 0.005$ is presented in Figs. 3 and 4.

Third, to provide further assurance for our numerical results, we estimate the energy balance for resistive wall modes. The variational principle corresponding to the Euler-Lagrange equation of Eq. (3) is

$$\delta W_{\rm rot} = \sum\left[\xi_\psi^*(x^2 - n^2\Omega^2)\frac{d\xi_\psi}{dx}\right]_{-\delta}^{\delta}$$
$$\approx -i\sum 4\pi n\Omega|\xi_\psi^l|^2, \qquad (5)$$

where ω_r and γ_p have been set to zero, which is a reason-

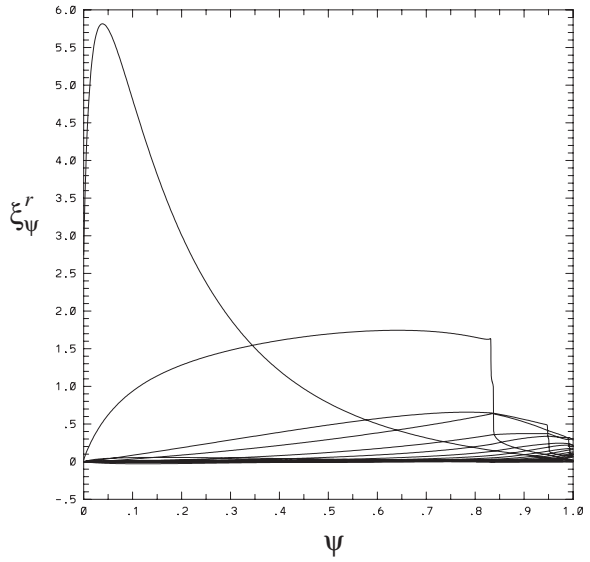

FIG. 3. Real part of the RWM eigenmode for normalized rotation frequency $\Omega = 0.005$.

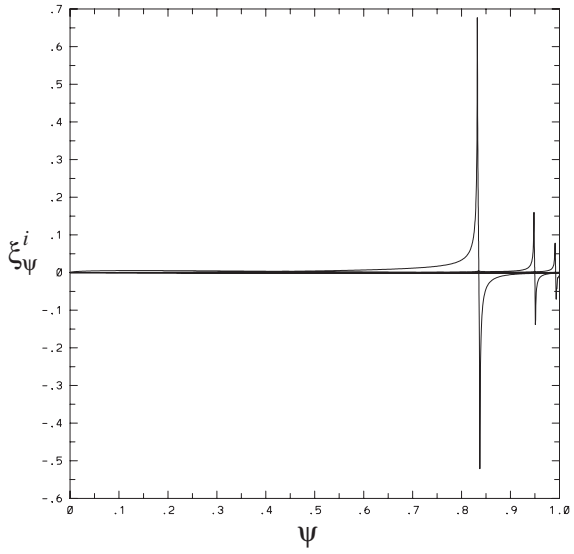

FIG. 4. Imaginary part of the RWM eigenmode for the same parameters as in Fig. 3.

able approximation for resistive wall modes, δ is the separation between the twin resonances, and the summation is over all MHD mode rational surfaces.

To estimate the magnitude of $\delta W_{\rm rot}$ in Eq. (5), let us compare it to the no-wall and zero rotation energy, δW_∞, which can be computed numerically. For the equilibrium we investigated, we find $\delta W_\infty = -2.7 \times 10^{-3}$. For low n modes in general, the average magnetic well can be used as an estimate for δW_∞,

$$\delta W_\infty \sim -(R/a)\beta\Delta|\xi_\psi|^2 + \delta W_v, \tag{6}$$

where R/a is the aspect ratio and Δ is the Grad-Shafranov shift. The vacuum energy δW_v is positive and partly cancels the negative plasma energy in the first term on the right-hand side of Eq. (6). The estimate in Eq. (6) is consistent with our numerically calculated value. Comparing Eqs. (5) and (6), one can see that $\delta W_{\rm rot}$ is comparable to δW_∞ when the normalized rotation frequency Ω is a few percent, as long as the ratio of the large solution ξ_ψ^l to the total solution ξ_ψ is finite. This ratio has to be determined numerically. Nevertheless, inspecting Eq. (4), one can see that the small solution is symmetric with respect to $x = 0$, while the large solution is not. Since low-n modes are radially broad, they are usually asymmetric around the rational surface and therefore a considerable amount of the large solution can be anticipated.

Having estimated the magnitude of $\delta W_{\rm rot}$, we proceed to demonstrate its stabilization effect. Similar to the method in Ref. [7], the resistive-wall-mode growth rate can be estimated as follows:

$$\gamma\tau_w \sim -\frac{\delta W_\infty \delta W_b + |\delta W_{\rm rot}|^2 - i|\delta W_{\rm rot}|(\delta W_b - \delta W_\infty)}{|\delta W_b + \delta W_{\rm rot}|^2}, \tag{7}$$

where τ_w is the resistive wall magnetic diffusion time, and δW_b is the system energy with perfectly conducting wall at b and no rotation. From Eq. (7), one can see that the imaginary $\delta W_{\rm rot}$ contributes to the stabilization. Note that $\delta W_b = 0$ at the critical wall position $b = 1.53$. From Eq. (7) one can see that the stabilization window should open from the vicinity of the critical wall position and ends at smaller b since δW_b increases as b decreases. This feature is exhibited in Fig. 1. Equation (5) shows that $\delta W_{\rm rot}$ is proportional to 2Ω. Therefore, the rotation stabilization should depend monotonically on Ω, which is seen in Fig. 2.

In summary, we have found that the resistive wall modes can be stabilized by the toroidal plasma rotation of low Mach number, without any contribution from wave-particle resonances. The sole stabilization mechanism comes from the shear-Alfvén MHD resonance. Since plasma rotation in the current ITER design has low Mach number, our result indicates a promising stabilization mechanism for ITER. The achievement of this result is credited to the small-growth-rate numerical scheme and the adaptive shooting method in the AEGIS code to resolve the Alfvén continuum damping. Our current investigation has focused on the rotation frequency regime where the particle-wave resonance is excluded, in order to isolate the Alfvén continuum damping effect and to address the parameter domain applicable to ITER. Nevertheless, even if the sound wave or kinetic resonances were present, the magnitude of the singular layer contribution revealed in our calculation indicates that not only the bulk plasma, but also the singular layers, contribute significantly to the stabilization of the resistive wall modes.

We are grateful to J. W. Van Dam for encouragement and advice with AEGIS work. We are also indebted to A. Turnbull for his help in benchmarks with GATO. We also thank H. Berk and F. Waelbroeck for helpful discussions. This research was supported by the Office of Fusion Energy Science of the U.S. Department of Energy under Grant No. DE-FG02-04ER54742.

*Electronic address: lzheng@mail.utexas.edu

[1] J. P. Freidberg, *Ideal Magnetohydrodynamics* (Clarendon, Oxford, 1987).
[2] E. J. Strait *et al.*, Phys. Rev. Lett. **74**, 2483 (1995).
[3] A. M. Garofalo *et al.*, Phys. Rev. Lett. **82**, 3811 (1999).
[4] S. A. Sabbagh *et al.*, Phys. Plasmas **9**, 2085 (2002).
[5] A. Bondeson and D. J. Ward, Phys. Rev. Lett. **72**, 2709 (1994).
[6] D. J. Ward and A. Bondeson, Phys. Plasmas **2**, 1570 (1995).
[7] R. Betti and J. P. Freidberg, Phys. Rev. Lett. **74**, 2949 (1995).
[8] B. Hu and R. Betti, Phys. Rev. Lett. **93**, 105002 (2004).
[9] R. Fitzpatrick and A. Aydemir, Nucl. Fusion **36**, 11 (1996).
[10] J. M. Finn, Phys. Plasmas **2**, 3782 (1995).
[11] A. Bondeson and H. X. Xie, Phys. Plasmas **4**, 2081 (1997).
[12] A. Bondeson, Y. Q. Liu, D. Gregoratto, C. M. Fransson, and Y. Gribov, Plasma Phys. Controlled Fusion **45**, A253 (2003).
[13] R. Aymar, P. Barabaschi, and Y. Shimomura, Plasma Phys. Controlled Fusion **44**, 519 (2002).
[14] M. S. Chu, J. M. Greene, W. Ling, A. D. Turnbull, H. L. Berk, and M. N. Rosenbluth, Phys. Plasmas **1**, 1214 (1994).
[15] L.-J. Zheng and M. Kotschenreuther, J. Comput. Phys. (to be published).
[16] F. Waelbroeck and L. Chen, Phys. Fluids B **3**, 601 (1991).
[17] L.-J. Zheng and M. Tessarotto, Phys. Plasmas **5**, 1403 (1998).
[18] A. B. Mikhalovskii and V. S. Tsypin, Fiz. Plazmy **9**, 147 (1983) [Sov. J. Plasma Phys. **9**, 91 (1983)].
[19] L. C. Bernard, F. J. Helton, and R. W. Moore, Comput. Phys. Commun. **24**, 377 (1981).